The magnetic, electrical transport and magnetoresistance properties of epitaxial $La_{0.7}Sr_{0.3}Mn_{1-x}Fe_xO_3$ (x = 0-0.20) thin films prepared by pulsed laser deposition

2001 J. Phys.: Condens. Matter 13 4033

(http://iopscience.iop.org/0953-8984/13/18/312)

INSTITUTE OF PHYSICS PUBLISHING JOURNAL OF PHYSICS: CONDENSED MATTER

J. Phys.: Condens. Matter **13** (2001) 4033–4047 www.iop.org/Journals/cm PII: S0953-8984(01)19856-5

The magnetic, electrical transport and magnetoresistance properties of epitaxial $La_{0.7}Sr_{0.3}Mn_{1-x}Fe_xO_3$ (x = 0–0.20) thin films prepared by pulsed laser deposition

Q Huang[1], **Z W Li, J Li and C K Ong**

Centre for Superconducting and Magnetic Materials and Department of Physics, National University of Singapore, Lower Kent Ridge Road, 119260, Singapore

E-mail: scip8203@nus.edu.sg (Q Huang)

Received 18 February 2001

Abstract

High-quality epitaxial $La_{0.7}Sr_{0.3}Mn_{1-x}Fe_xO_3$ (LSMFO) thin films have been successfully prepared on $SrTiO_3$ single-crystal substrates by pulsed laser deposition. No structural changes were observed for $x \leqslant 0.12$. For $x = 0.2$, an elongation in the a-axis direction was identified. An antiferromagnetic arrangement of Fe and Mn ions over the whole Fe-doping region and a canted spin structure at $x \geqslant 0.12$ were observed. Unlike the case for the bulks, only one resistivity peak was observed for the epitaxial films. This shows that one of the two resistivity peaks for polycrystalline LSMFO bulks has its origin in grain boundaries. The effect of Fe doping can be attributed to a combination of doping disorder, Fe–Mn superexchange interactions and a site-percolation mechanism, which suppress the metallic conduction and ferromagnetism. In epitaxial LSMFO thin films, extrinsic magnetoresistance (MR) related to grain boundary effects was excluded. The intrinsic MR is gradually enhanced with increasing Fe concentration. For the film with $x = 0.12$, a fairly large MR = 12% was observed in a small field of 4 kOe at 145 K. For those films, the resistivity above T_c (the ferromagnetic Curie temperature) follows the Emin–Holstein model for small polarons. The polaron activation energy is enhanced due to weakening of the local double-exchange ferromagnetism by Fe doping. The fitting results indicate that the lattice polarons are magnetic in nature and that non-nearest-neighbour polaron hopping exists. The resistivity below T_p (the resistivity peak temperature) follows an empirical relation, $\rho(T, H) = \rho_0 + \rho_2(H)T^2 + \rho_{7.5}(H)T^{7.5}$. It is found that the MR arises mainly from the suppression of $T^{7.5}$-terms. The enhanced MR can be attributed to the suppression of the enhanced magnetic scattering and polaron scattering under an external field.

[1] Fax: (65)777-6126.

0953-8984/01/184033+15$30.00

1. Introduction

Recent research on the mixed-valence manganites ($La_{1-y}A_yMnO_3$, A = Ca, Sr, Ba) has focused on the enhancement of the magnetoresistance (MR) [1]. Two kinds of approach have been utilized. The first is that of using ion substitution [2] to adjust the bonding length/angle of the Mn–O–Mn network, thus affecting the double-exchange (DE) process [3]. This intrinsic MR enhancement occurs near the Curie temperature T_c. The second is that of introducing a second phase such as grain boundaries (GB). For samples including GB, the large LFMR (low-field MR) at low temperatures was attributed to the spin-dependent transport across the GB [4, 5]. The high-field MR was related to the spin disorder or non-collinear magnetism at the GB [6–9]. This extrinsic phenomenon is absent for single crystals and high-quality epitaxial films. Recently, using the first approach, Uehara *et al* [10] have shown that the MR enhancement for the (LaPrCa)MnO_3 system is related to inhomogeneous conduction, as the system is phase separated into a mixture of insulating and metallic regions. The chemical pressure modulates the subtle balance between the insulating/metallic states. For the second approach, inhomogeneous two-phase-mixed microstructures, where the ferromagnetic (FM) metal and insulating phase coexist, have been utilized to enhance the low-field MR [11–13]. It seems that different research branches are converging toward a coherent physical picture that is related to the inhomogeneous conduction. It is therefore of interest to study the MR properties for typical inhomogeneous systems, such as the Fe-doped manganites. Previously, Ahn *et al* [14, 15] found that Fe doping favours insulating conduction and antiferromagnetism opposing the DE ferromagnetism in $La_{1-y}Ca_yMn_{1-x}Fe_xO_3$. On the basis of electronic structure considerations, these authors argued that Fe^{3+} does not participate in the DE process. Consequently, the Mn–O–Mn metallic network and the Fe–O–Mn insulating network coexist at low temperatures. Leung *et al* [16] studied the Mössbauer effect of $La_{1-y}Pb_yMn_{1-x}Fe_xO_3$ and found antiferromagnetic (AFM) coupling between Fe and Mn ions. Cai *et al* [17] found the occurrence of spin-glass behaviour for $La_{0.67}Ca_{0.33}Mn_{0.9}Fe_{0.1}O_3$ and suggested competition between the ferromagnetic and antiferromagnetic clusters. Ogale *et al* [18] discovered the occurrence of a localization–delocalization transition at a critical Fe concentration in $La_{0.75}Ca_{0.25}Mn_{1-x}Fe_xO_3$. It was argued that a quasi-particle of finite dimension $\sim$ three unit cells should be associated with the carrier transport in the system.

The studies on the Fe-doped manganites have focused on the $La_{1-y}Ca_yMnO_3$ system. Reports on Fe-doped $La_{1-y}Sr_yMnO_3$ are few [19, 20]. More importantly, as far as we know, all research on Fe-doped manganites has been on polycrystalline samples. In such samples, GB not only contribute to the resistivity, as shown by microwave measurements [21], but also play an essential role in modulating the MR by adding an extrinsic term to the MR besides the intrinsic one arising from the grains [4–9]. The resistivity and MR response in these polycrystalline manganites are mixtures of contributions from both the grains and the GB. However, high-quality epitaxial thin-film samples allow us to minimize the effects of GB, and extract the effects of Fe doping with high reliability. In particular, data obtained from epitaxial films will facilitate a quantitative analysis of the resistivity and MR of Fe-doped manganites, which is still lacking at present. In this paper, the microstructural, magnetic, electrical transport and MR properties of epitaxial $La_{0.7}Sr_{0.3}Mn_{1-x}Fe_xO_3$ (LSMFO) thin films with $x = 0.0$–0.20 have been systematically studied.

2. Experiment

A pulsed laser deposition (PLD) experiment was performed by utilizing a Lambda Physik KrF excimer laser 248 nm in wavelength, 30 ns in pulse width and 5 Hz in repetition rate. Ceramic

LSMFO discs with $x = 0.00$, 0.02, 0.05, 0.08, 0.12 and 0.20 were chosen as targets. The targets were made using the standard ceramic synthesis techniques. High-purity (>99.5%) oxide powders of La_2O_3, SrO, MnO_2 and Fe_2O_3 were repeatedly reacted in air at 1250 °C for several days. The LSMFO films were deposited using an optimized set of deposition parameters [22, 23]. (001)-oriented $SrTiO_3$ (STO), $5 \times 10 \times 0.5$ mm^3 in size, was chosen as the substrate. The laser frequency was 1.8 J cm^{-2}. The substrate temperature was 680 °C and the oxygen ambient pressure was 0.5 mbar. The deposition chamber was pumped to a base vacuum of 1.0×10^{-6} mbar before deposition. The films were deposited at a rate of about 60 Å min^{-1} with a typical thickness of 2500 Å. The as-deposited films were post-annealed for 30 min at 680 °C in an O_2 pressure of 400 mbar prior to cooling down to room temperature at a rate of 15 K min^{-1}.

The crystal structures of these targets and films were checked by x-ray diffraction (XRD) using a Phillips diffractometer with Cu Kα radiation. The film thickness was measured by an Alpha-step 500 surface profiler and confirmed by an atomic force microscope. The electro-transport properties of the films were evaluated using a four-probe method. The magnetoresistance was measured in an AC magnetic field 4.0 kOe in magnitude and 0.01 Hz in frequency. The direction of the magnetic field was parallel to the current direction. The magnetic properties were measured using an Oxford superconducting vibrating-sample magnetometer (VSM). In order to correct for the diamagnetic effects of the substrates, their magnetization curves were measured before film deposition. The temperature ranges were 77–360 K for the electrical measurements and 77–300 K for the magnetic measurements.

3. Results

3.1. Microstructure

XRD patterns showed that all of the sintered LSMFO targets are single phase without detectable secondary phase or impurity. All of the reflection lines are successfully indexed with a rhombohedral ($R\bar{3}c$) ABO_3-type perovskite structure using the program DICVOL91 [24]. For the targets with $x = 0$–0.12, the lattice parameters a and c, the ratio c/a and the volume V are constant within the experimental errors: $a = 5.52$ Å, $c = 6.69$ Å, $c/a = 1.212$ and $V = 177$ Å^3 (see table 1). From crystallography, we know that if $c/a = \sqrt{6}$, the $R\bar{3}c$ system becomes cubic. For LSMFO, $2c = 2.424a \approx \sqrt{6}a$; thus it can be treated as a pseudo-cubic

Table 1. The characteristics of $La_{0.7}Sr_{0.3}Mn_{1-x}Fe_xO_3$. a and c are lattice parameters for the bulks. M_s is the saturation magnetization (measured at 77 K). T_c is the magnetic transition temperature, T_p the insulator–metal transition temperature. MR_{MAX} and T_{MR} are the maximum MR and the corresponding temperature, respectively.

x:	0.00	0.02	0.05	0.08	0.12	0.20
a (Å)	5.521(2)	5.523(2)	5.521(2)	5.523(2)	5.525(1)	5.540(2)
c (Å)	6.693(3)	6.691(3)	6.690(3)	6.694(4)	6.693(2)	6.692(5)
$2c/\sqrt{6}a$	0.99	0.989	0.99	0.99	0.989	0.987
V (Å^3)	176.7	176.8	176.7	176.9	177.0	177.9
M_s (emu cm^{-3})	561	492	451	338	171	127
T_c (K)	360[a]	> 300	320[a]	258	204	166
T_p (K)	> 360	332	310	230	138	< 77
T_{MR} (K)	324	300	280	189	145	N/A
MR_{MAX}	5.0%	7.4%	7.8%	9.3%	12%	N/A

[a] From references [20, 28].

structure with the lattice constant $a_c \approx 3.9$ Å. The XRD patterns of the targets with $x = 0.0$ and 0.12 are presented in figure 1(a). The (101) and (202) planes in the rhombohedral structure correspond to the (001) and (002) planes in the pseudo-cubic structure.

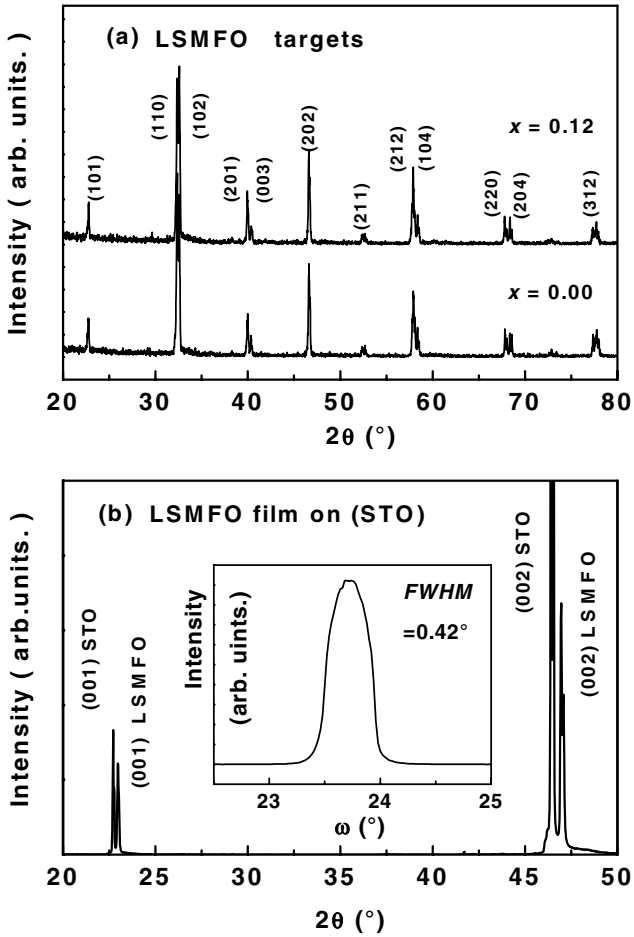

Figure 1. The XRD θ–2θ patterns of $La_{0.7}Sr_{0.3}Mn_{1-x}Fe_xO_3$. (a) Ceramic targets and (b) the thin film with $x = 0.12$. Inset: the ω-scan.

The x-ray θ–2θ scan showed that all of the LSMFO thin films on STO are single phase with (001)-oriented cubic perovskite structure. The full widths at half-maximum (FWHM) of the ω-scans on the (002) planes are around 0.45°, which indicates the high crystalline quality of the films. As an example, the XRD pattern of the LSMFO thin film with $x = 0.12$ is presented in figure 1(b). The FWHM of its ω-scan is only 0.42°, as shown in the inset. This can be attributed to the small lattice mismatch (<1%) between LSMFO and STO. In comparison, a preliminary ω-scan on the (002) planes of the films deposited on $LaAlO_3$ produced a typical FWHM around 0.85°, because $LaAlO_3$ has a larger lattice mismatch (>2%) with LSMFO. For different Fe concentrations with $x = 0$–0.12, the $d_{(002)}$-reflections have the same value of 1.937(1) Å. For $x = 0.20$, $d_{(002)}$ is equal to 1.9417 Å, slightly larger than that for the other films. These values are in agreement with the changes of lattice parameters in the bulk target materials.

3.2. Magnetic properties

Figure 2 presents the reduced magnetization, M/M_s, of LSMFO thin films as a function of the reduced temperature, T/T_c, at a field of 4 kOe. The saturation magnetizations, M_s, and the ferromagnetic Curie temperatures, T_c, of the films are listed in table 1. The values of the saturation magnetization, especially for the films with $x = 0.12$ and 0.20, are obtained from the law of approach to saturation:

$$M = M_s(1 - A/H + B/H^2) + \chi_p H \tag{1}$$

where M_s is the saturation magnetization and χ_p is the high-field susceptibility. A decrease in the magnetization with Fe doping implies an AFM arrangement of the Fe and Mn ions. The AFM Fe–O–Mn interaction has been identified by Mössbauer spectroscopy with an applied magnetic field in (LaPb)MnO_3 [16] and (LaCa)MnO_3 [17] systems. The AFM superexchange interaction weakens the FM DE between the Mn ions and leads to a decrease in T_c. For LSMFO thin films, T_c significantly reduces from ~360 K for $x = 0$ to 166 K for $x = 0.20$. Furthermore, in figure 2, the M/M_s–T/T_c curves drop rapidly with Fe doping; this also means that the DE is weakened by the AFM interaction.

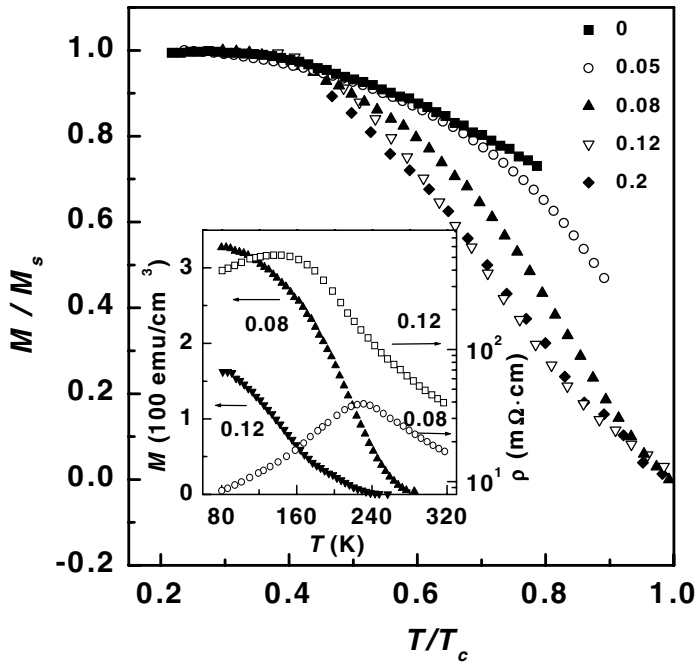

Figure 2. The reduced magnetization of $La_{0.7}Sr_{0.3}Mn_{1-x}Fe_xO_3$ thin films as a function of temperature at a field of 4 kOe. Inset: the evolution of magnetization M with temperature for $x = 0.08$ and 0.12. The resistivity data are replotted on the right-hand-side scale for comparison.

Another interesting magnetic characteristic is the high-field susceptibility, χ_p, as shown in the magnetization curves in figure 3. For $x \leqslant 0.08$, χ_p is negligible and the magnetization rapidly increases to saturation in a small field. However, when $x \geqslant 0.12$, the magnetization is not saturated even in a field as high as 50 kOe. According to equation (1), the values of χ_p are 6.87×10^{-4} emu cm^{-3} Oe^{-1} and 8.79×10^{-4} emu cm^{-3} Oe^{-1} for the films with $x = 0.12$ and 0.20, respectively. This suggests that a non-collinear magnetic structure (spin canting) occurs for the films with $x \geqslant 0.12$.

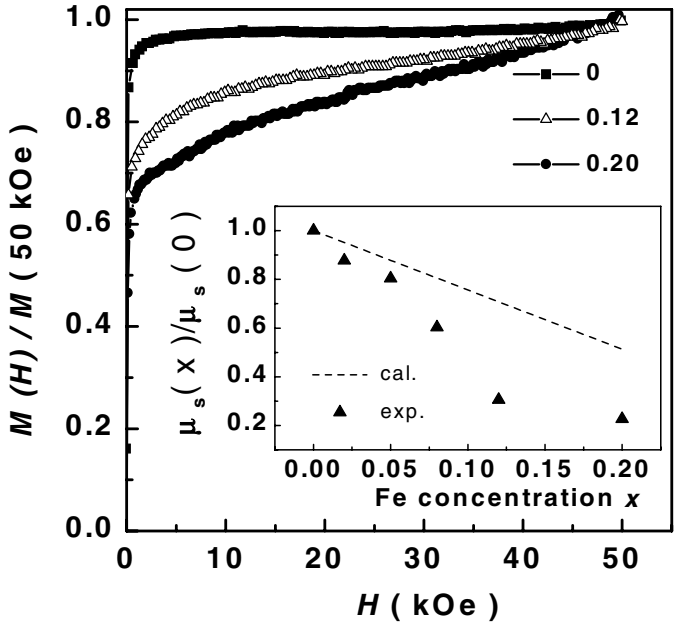

Figure 3. The magnetization curves at 77 K for $La_{0.7}Sr_{0.3}Mn_{1-x}Fe_xO_3$ thin films. The inset shows the reduced saturation magnetic moment $\mu_s(x)/\mu_s(0)$ per formula unit versus Fe concentration x, which is measured in a field of 50 kOe. The dashed line indicates the theoretical prediction of equation (2).

On the basis of the single-ion model with an AFM arrangement of the Mn and Fe ions, the theoretical values of the saturation magnetic moment per formula unit μ_{th} can be expressed as

$$\mu_{th} = (\mu_{Mn^{3+}})(n_{Mn^{3+}}) + (\mu_{Mn^{4+}})(n_{Mn^{4+}}) - (\mu_{Fe^{3+}})(n_{Fe^{3+}}) \tag{2}$$

where $\mu_{Mn^{3+}}$ $(4\mu_B)$, $\mu_{Mn^{4+}}$ $(3\mu_B)$, $\mu_{Fe^{3+}}$ $(5\mu_B)$ are the spin moments (the orbital contribution is quenched) and $n_{Mn^{3+}}$, $n_{Mn^{4+}}$, $n_{Fe^{3+}}$ are the ionic numbers of the Mn^{3+}, Mn^{4+} and Fe^{3+} ions. In the inset of figure 3, the reduced saturation magnetic moment per formula unit $\mu_s(x)/\mu_s(0)$ and its theoretical value are plotted against Fe concentration x. The experimental data are close to the theoretical values for low Fe doping, which confirms the AFM arrangement between the Fe and Mn ions. The experimental value drops much faster than the predicted one for high Fe doping because of the canted spin structure, which can be attributed to the competition between ferromagnetic and antiferromagnetic interactions [25]. When the Fe-doping concentration is high, a given Fe ion will have both Fe ions and Mn ions as its nearest neighbours. Due to the competition between Fe–Fe, Fe–Mn and Mn–Mn magnetic interactions, the spins of Fe and Mn ions will deviate to misaligned directions and this will result in a canted structure.

3.3. Electrical transport

The resistivities, ρ, of the LSMFO films at zero field are shown in figure 4. For the undoped film, ρ is replotted on the right-hand-side expanded scale. The metallic conduction over the whole measurement temperature range (77–360 K) indicates that the insulating–metallic transition temperature, T_p, is higher than 360 K, which is in good agreement with $T_p \sim 375$ K for stoichiometric $La_{0.7}Sr_{0.3}MnO_3$ (LSMO) [26]. The value of ρ at 77 K is 0.38 mΩ cm, comparable to the residual resistivity of 0.1 mΩ cm for LSMO single crystal [27] and

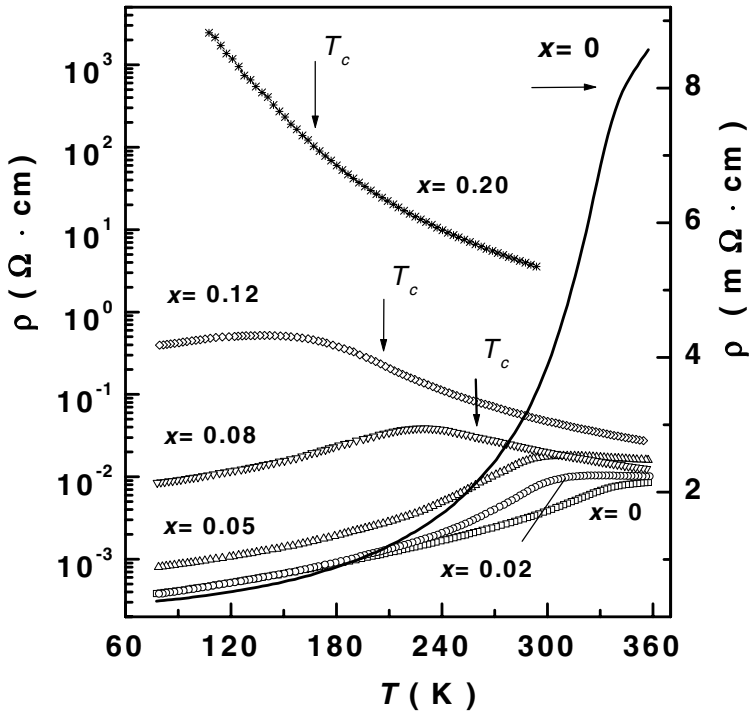

Figure 4. The resistivities of $La_{0.7}Sr_{0.3}Mn_{1-x}Fe_xO_3$ thin films as functions of temperature at zero field. The resistivity of the undoped sample is replotted on the right-hand-side expanded scale. The ferromagnetic Curie temperatures T_c are indicated by arrows.

0.15 mΩ cm for $La_{0.67}Sr_{0.33}MnO_3$ MOCVD thin films [28]. This value is much lower than that of 12 mΩ cm for the polycrystalline sample [29]. Furthermore, the epitaxial film showed a much sharper transition. $\rho(T_p)/\rho(77\ \mathrm{K})$ is larger than 22 for the film as compared to 2.5 for the polycrystalline bulk [29].

As x changes from 0 to 0.20, a tremendous change of ρ of over six orders in magnitude is observed at 77 K. For the sample with $x = 0.02$, the ρ–T curve at low temperature remains almost consistent with that for the undoped sample. Further Fe doping leads to a rapid increase in ρ. The value of ρ at 77 K increases by half an order and more than one order of magnitude for the films with $x = 0.05$ and 0.08, respectively, as compared to the film with $x = 0$. With increasing Fe doping, T_p for the films shifted to lower temperatures, which are 332, 310, 230, 138 K for the films with $x = 0.02$, 0.05, 0.08 and 0.12, respectively, as shown in table 1. The film with $x = 0.20$ exhibits a typical insulator behaviour. It is worth noting that Xianyu *et al* [20] have just reported that two adjacent peaks exist in ρ–T curves for LSMFO bulks with $x = 0$–0.10. However, for the epitaxial films, only one resistivity peak was observed. This shows that the second peak has its origin in GB for the polycrystalline bulk.

3.4. Magnetoresistance at a low field

For the films with $x \leqslant 0.12$, the linear ρ–H hysteresis loops were recorded at all temperatures. In figure 5, the reduced resistivity, $\rho(H)/\rho(0)$, is plotted against the external field, H, at the temperature T_{MR}, which corresponds to the maximum MR. The temperatures T_{MR} are 324,

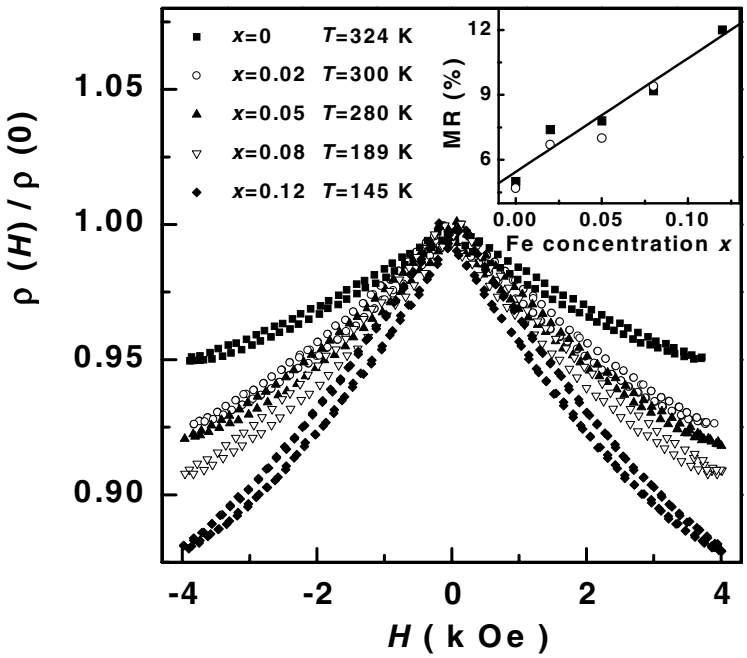

Figure 5. $\rho(H)/\rho(0)$ is plotted against the external field at the temperatures where MR reaches its maximum values. Inset: the maximum MR versus the Fe-doping concentration. Solid squares show the experimental data. The open circles show the calculated values according to equation (8).

300, 280, 189 and 145 K for the films with $x = 0$, 0.02, 0.05, 0.08 and 0.12, respectively. The linear ρ–H response and $T_{MR} \sim T_p$ suggest that the intrinsic MR is dominant. However, the contribution from the extrinsic MR [4–9], which is related to GB, can be excluded because the extrinsic MR occurs at low temperatures and should exhibit a non-linear response to H at low field.

As shown in figure 5 and its inset, the maximum MR is gradually enhanced with increasing Fe concentration. For the film not doped with Fe, the value of the MR is only 5%. However, for the film with $x = 0.12$, a fairly large MR of 12% is observed at 145 K. Here, the value of the MR is defined as MR $= [\rho(H = 0) - \rho(H = 4\ \text{kOe})]/\rho(H = 0)$. This is in agreement with the MR enhancement observed near T_c in the LSMFO polycrystalline bulks [20]. However, in contrast to the bulk materials, the epitaxial films have no MR enhancement at low temperatures (far below T_c), as shown in figure 6. It is evident that the GB in the bulk materials play a dominant role in the spin-polarized transportation at low temperatures.

4. Discussion

4.1. Effects of Fe doping: disorder, superexchange and site percolation

Jonker revealed the existence of Fe^{3+}, Mn^{3+} and Mn^{4+} ions in $La_{0.85}Ba_{0.15}Mn_{1-x}Fe_xO_3$ for $x < 0.85$ [30]. Mössbauer measurements established that the Fe^{3+} only occupies the Mn site of $La_{0.83}Sr_{0.17}Mn_{0.98}{}^{57}Fe_{0.02}O_3$ [31]. Thus, the nominal stoichiometry for our samples can be written as $La^{3+}_{0.7}Sr^{2+}_{0.3}Mn^{3+}_{0.7-x}Fe^{3+}_{x}Mn^{4+}_{0.3}O_3$. The effects of Fe doping can be summarized as follows:

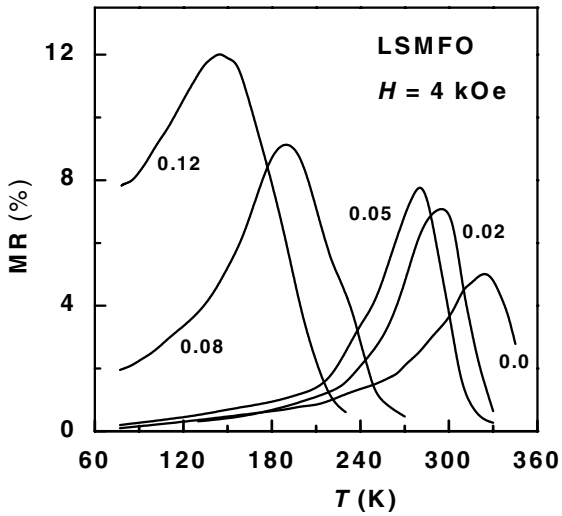

Figure 6. The magnetoresistance, MR $= [\rho(H = 0) - \rho(H = 4\ \text{kOe})]/\rho(H = 0)$, is plotted against temperature for LSMFO films.

(1) According to Ahn *et al* [14] the top of the Fe e_g band is almost located at the bottom of the Mn e_g band, just with an overlap of less than 3%. Intrinsically, Fe^{3+} cannot act as the double-exchange partner with Mn^{4+}, as Fe ions act as trapping centres and block the conduction path of e_g electrons.
(2) DE is partially suppressed in LSMFO. Instead, a super-exchange coupling (SE) is established between Fe and Mn ions and the AFM appears, as verified in section 3.2.
(3) The Fe^{3+} act as a local anti-Jahn–Teller distortion force, affecting the bonding angles/length of the neighbouring Mn–Mn channel because Fe^{3+} is a non-Jahn–Teller ion.
(4) The average valence of the Mn–Fe–Mn network is 3.2+, higher than that of Fe^{3+}. In the fluctuating Mn^{3+}/Mn^{4+} environment, the local electrostatic energy forces electrons to reside at the Mn^{4+} state which neighbours with Fe^{3+} for a longer time than at that without Fe^{3+} as neighbour [18].
(5) The randomness of the Fe substitution results in various near-neighbour configurations of Mn and Fe ions, therefore causing a distribution of the Mn-site energies.

In fact, factors (3)–(5) constitute non-magnetic energy fluctuations at the Mn sites, which have been theoretically considered in disorder models [32–34]. Within the disorder models, the Hamiltonian is composed of two terms: one is the DE energy and the other is the random on-site (Mn-site) energy from the disorder. The random on-site energy tends to localize the charge carriers and to decrease T_p. The models predict that ferromagnetism and insulating-like conductivity can coexist in the sample with a high degree of disorder. This is consistent with our experimental observation for the LSMFO films with $x \geqslant 0.08$, as shown in figure 4, where the insulating conductivity was observed below T_c. Furthermore, Fe doping is doing more than just causing disorder: it changes not only the magnitude, but also the sign of the magnetic interactions. In particular, when the Fe concentration x is high, the reduction of the number of available Mn–O–Mn channels must be considered. Taking the film with $x = 0.12$ as an example, the average Fe–Fe distance is $x^{-1/3} \sim 2$ unit cells and a site-percolation mechanism sets in. Consequently, a slower decrease of its resistivity at low temperatures was observed, which is an indication of a percolation-like crossover in resistivity. In conclusion, the Fe-doping

effect in LSMFO can be viewed as a combination of doping disorder, Fe–Mn superexchange interactions and a site-percolation mechanism, which suppress the metallic conduction and ferromagnetism, as verified in section 3.

4.2. Polaron hopping and insulating-like conductivity

The resistivity data for above T_c can be fitted using the nearest-neighbour small-polaron-hopping model in the Emin–Holstein theorem, which gives [35, 36]

$$\rho = BT \exp\left(\frac{W_p}{kT}\right) \tag{3}$$

with

$$B = g_d k_B / ne^2 a^2 \nu_0 \tag{4}$$

where W_p is the activation energy, B the resistivity coefficient, g_d the lattice geometry factor, k_B the Boltzmann constant, n the polaron concentration, e the electronic charge, a the hopping distance and ν the longitudinal optical phonon frequency. To get B and W_p, the experimental data for the films were plotted as $\ln(\rho/T)$ against $1/T$ and fitted using a linear regression method. The fitted lines are presented in figure 7 and the corresponding fitting parameters are listed in table 2. Note here that the changes in W_p and B are all substantially larger than the fitting errors, thus giving us a reasonable basis for discussion.

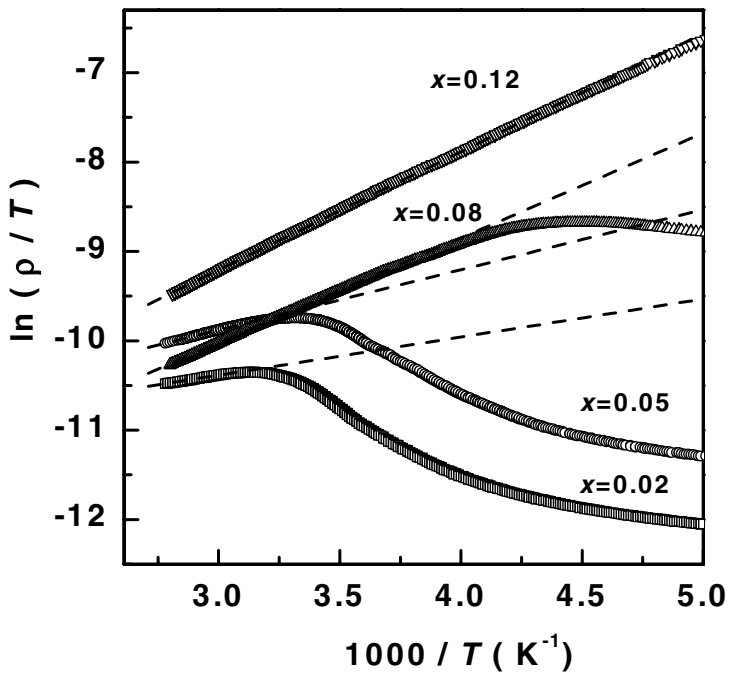

Figure 7. $\ln(\rho/T)$ is plotted against the inverse temperature for $La_{0.7}Sr_{0.3}Mn_{1-x}Fe_xO_3$ ($x \leqslant 0.1$). The dashed lines are fits of the adiabatic small-polaron model.

As x increases, W_p increases monotonically. This can be attributed to the magnetic nature of the lattice polaron. The concept of the magnetic polaron has satisfactorily explained some neutron diffraction [37–39], magnetic susceptibility [40] and electron spin-resonance (ESR)

Table 2. Fitting parameters for the resistivity data. When $T > T_c$, the resistivity data are fitted using the small-polaron model, which gives $\rho = BT\exp(W_p/kT)$; when $T < T_p$, the resistivity data are fitted using the simple empirical relation $\rho(T, H) = \rho_0 + \rho_2(H)T^2 + \rho_{7.5}(H)T^{7.5}$. The numbers in brackets represent the standard errors for the last effective digits.

x	0.00	0.02	0.05	0.08	0.12	0.20
W_p (meV)	N/A	39.3(1)	61.6(1)	101.64(5)	114.60(5)	134.20(4)
B (10^{-6} Ω cm K^{-1})	N/A	7.80(2)	6.01(2)	1.29(1)	1.85(1)	61.2(2)
ρ_0 (mΩ cm)	0.315(9)	0.48(4)	0.66(5)	5.84(2)	295(8)	N/A
$\rho_2(0)$ (10^{-8} Ω cm K^{-2})	1.55(3)	0.37(9)	2.82(8)	39.2(5)	$1.1(2) \times 10^3$	N/A
ρ_2(4 kOe) (10^{-8} Ω cm K^{-2})	1.57(3)	0.40(6)	2.82(8)	37.5(5)	$1.5(1) \times 10^3$	N/A
$\rho_{7.5}(0)$ (10^{-21} Ω cm $K^{-7.5}$)	0.603(2)	2.02(3)	4.44(4)	54(1)	$7.5(2) \times 10^3$	N/A
$\rho_{7.5}$(4 kOe) (10^{-21} Ω cm $K^{-7.5}$)	0.562(5)	1.87(3)	4.04(4)	33(1)	$1.4(2) \times 10^3$	N/A

[41] experiments. It is suggested that a complex short-range magnetic order coupled with the lattice and related to the charge dynamics persists far above T_c. The polarons are magnetically dressed, as DE is still effective in the vicinity of the trapped carriers. The magnetic nature of the polaron lowers its binding energy. Thus the magnetically dressed polaron has a lower binding energy than a pure lattice polaron. As shown in section 3.2, Fe doping weakens the local DE ferromagnetism, so the magnetic nature of the lattice polaron decays, causing W_p to increase.

The resistivity coefficient B as a function of x first decreases ($x = 0.02$ to 0.08) and then increases ($x = 0.08$ to 0.12) (table 2). It seems unlikely that v_0 changes sufficiently at the low-x level to account for the large variation of B. Therefore it is possible to attribute the variation of B to the change of n or a with x. In fact, replacement of Jahn–Teller Mn^{3+} ions with non-Jahn–Teller Fe^{3+} ions will lead to a decrease in polaron concentration n. Meanwhile, as the e_g shell of Fe^{3+} is fully filled, the charge carriers cannot pass through the Fe^{3+} sites due to strong Coulomb repulsion. Therefore, the Fe^{3+} act as barriers to the charge carriers. The carriers must detour or hop over these enhanced barriers due to Fe doping, so the average hopping distance a increases with x. When $x \leqslant 0.08$, the contribution from the growth of a with x dominates and causes B to decrease. However, a has an upper limit due to the finite activation energy of the polaron. When $x \geqslant 0.12$, the change of n overwhelms that of a, which makes na^2 drop even though a increases, causing B to increase. Here the increase of the average hopping distance, a, indicates that the polaron will hop further than the nearest-neighbour sites if there are enough on-site barriers caused by Fe doping. Consequently, the dominating transport process in LSMFO could be a combination of polaron nearest-neighbour hopping and non-nearest-neighbour hopping. Previously, similar hopping processes have also been reported in $La_{0.67}Ca_{0.33}Mn_{1-x}Ga_xO_3$ [36] and even in $La_{1-y}Ca_yMnO_3$ when the polaron concentration is high [42]. The origin of these phenomena was taken to be the on-site Coulomb repulsion and the polaron–polaron interactions.

4.3. Metallic conductivity and MR

Below T_c, one of the empirical relations between ρ and M for manganites is given by [43]

$$\rho(T, H) = \rho_m \exp(-M(T, H)/M_0) \tag{5}$$

where ρ_m and M_0 are fitting parameters. Equation (5) corresponds to a polaron hopping process due to the fact that if the polaron-hopping-type transport is relevant near T_c, it should be activated by the effective hopping interaction t_{eff}; that is, $\rho \propto \exp(-t_{eff})$, with $t_{eff} \propto M$. For the LSMFO films with $x < 0.12$, equation (5) fits the resistivity data near and below T_p

(150 K $< T <$ T_p) well, giving $\rho_m = 0.19$–$4.72\ \Omega$ cm and $M_0 = 0.80$–1.49 kG. However, it fails to fit the resistivity for $T < 150$ K. This indicates that polaron hopping is still prevalent near and below T_p for LSMFO thin films. Unlike the small polarons above T_c, as discussed in section 4.2, the polarons below T_p were suggested to be extended large polarons [26, 43].

On the other hand, the resistivity of LSMO and LCMO ($La_{0.67}Ca_{0.33}MnO_3$) at low temperatures ($T < T_c/2$) is well fitted using the equation [28, 44]

$$\rho(T, H) = \rho_0 + \rho_2 T^2 + \rho_{4.5}(H) T^{4.5} \tag{6}$$

where ρ_0 is the residual resistivity due to the temperature-independent scattering mechanism. The terms in T^2 and $T^{4.5}$ arise from electron–electron scattering and the electron–magnon scattering, respectively. Here, we found that the resistivity data for LSMFO can be well fitted using a simple empirical relation:

$$\rho(T, H) = \rho_0 + \rho_2(H) T^2 + \rho_{7.5}(H) T^{7.5} \tag{7}$$

where ρ_0, $\rho_2(H)$ and $\rho_{7.5}(H)$ are fitting parameters. The fitting parameters ρ_0, ρ_2 and $\rho_{7.5}$ were evaluated by best fitting the experimental data both at zero field and at $H = 4$ kOe. When fitting the data at $H = 4$ kOe, ρ_0 was kept the same as that in the case of $H = 0$. The fitted results are shown in figure 8 and the parameters are listed in table 2. The equation is similar to equation (6), except for the higher order in the third term. ρ_0 is the residual resistivity, which is related to the Fe doping but is independent of H and T. In the case of $H = 4$ kOe, $\rho_2(H)$ is almost independent of H, except for the film with $x = 0.12$. To explain the T^2-term, two mechanisms have been proposed. One is that of the theory of spin fluctuation [45]. The T^2-term is often observed for metallic ferromagnets and the coefficient [46] is usually about $10^{-11}\ \Omega$ cm K^{-2}. The other is that of the electron–electron scattering theory [47]. The coefficient of the T^2-term is about $10^{-8}\ \Omega$ cm K^{-2} for LSMO [28]. Therefore, our results, $\rho_2 \sim 10^{-8}\ \Omega$ cm K^{-2}, imply that the T^2-term may have its origin in the electron–electron scattering. In equation (6), the $T^{4.5}$-term is usually connected to electron–magnon scattering. Kubo and Ohata [48] have indicated that, according to the spin-wave approximation, the resistivity should vary as $T^{4.5}$ at low temperatures. For LSMFO systems, $T^{4.5}$-fitting cannot work well with the experimental data at $T > T_c/2$. However, using the $T^{7.5}$-fitting, the range of validity of equation (7) can be extended over the whole temperature range between 77 K and near T_p, as shown in figure 8. As shown in the inset of figure 8, the term $\rho_0 + \rho_2 T^2$ is responsible for the resistivity at low temperature and the term $\rho_{7.5} T^{7.5}$ is dominant near T_p. It is possible that the $T^{7.5}$-term originates partly from the polaron formation near T_p, since both the $T^{7.5}$-term and equation (5) fit the resistivity near T_p well. In fact, equation (5) can be expanded into a polynomial form to give higher-order T^n-terms. Future studies are needed to clarify this issue.

Finally, on the basis of equation (7), the magnetoresistance coefficients, MR, of LSMFO are given by

$$\mathrm{MR} = -\frac{\Delta\rho}{\rho} \approx \frac{(\rho_{7.5} - \rho_{7.5}(H))T^{7.5}}{\rho_0 + \rho_2 T^2 + \rho_{7.5} T^{7.5}}. \tag{8}$$

The inset of figure 5 shows the calculated values of MR (open circles) for various Fe-doping levels at $T = T_{\mathrm{MR}}$, which agree well with the experimental data. Interestingly, the maximum MR has a linear relationship with the Fe doping to a good approximation. This implies that MR is directly related to the Fe concentrations or, in other words, the change of magnetic properties caused by the Fe doping. For the LSMFO films, the Fe–O–Mn antiferromagnetic arrangements with Fe doping and the canting of moments for high Fe doping have been observed in section 3.2. Apparently, this causes additional magnetic scattering. On the other hand, Fe doping also enhances the polaron scattering above T_c (W_p increases) due to the

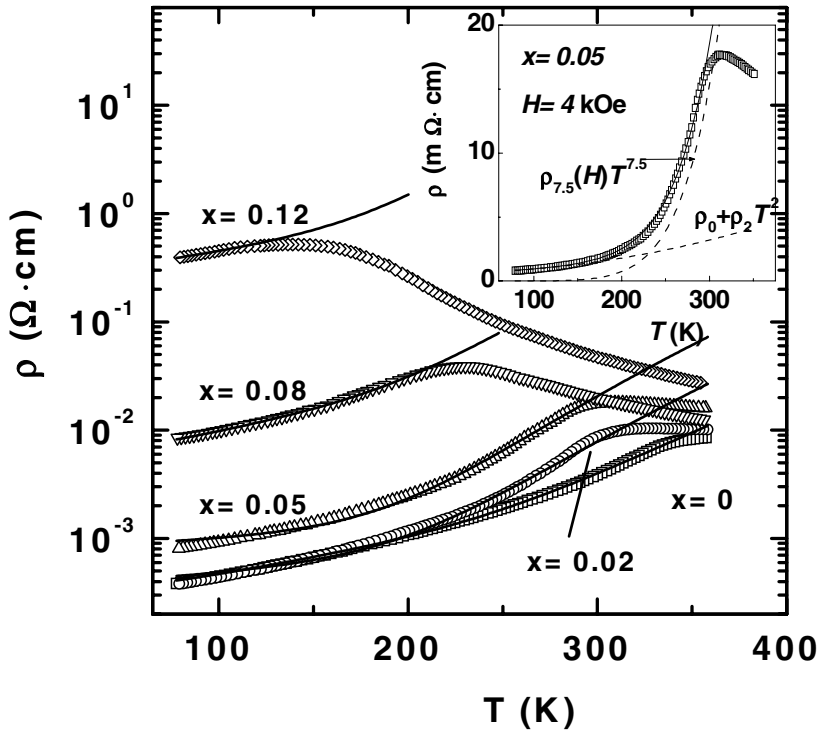

Figure 8. The zero-field resistivity of $La_{0.7}Sr_{0.3}Mn_{1-x}Fe_xO_3$ ($x \leqslant 0.1$) thin films as a function of temperature for various Fe-doping levels. The solid lines are fitted curves based on equation (7). Inset: the resistivity data for $x = 0.05$ under a field of 4 kOe. The dashed lines indicate the fitted components.

weakening of the local DE ferromagnetism, as verified in section 4.2. It is reasonable to assume that this picture is also applicable to the extended polarons just below T_p. Under an external magnetic field, the additional scattering on electrons will be suppressed. As a result, the MR values will increase with Fe doping.

5. Conclusions

The microstructure, magnetic and electrical transport properties of epitaxial LSMFO thin films have been systematically studied. No structural changes were observed for $x \leqslant 0.12$. An AFM arrangement of the Fe and Mn ions over the whole Fe-doping range and a canted spin structure at $x \geqslant 0.12$ were observed. Upon doping with Fe, the conductivity and the ferromagnetism were systematically lowered. In contrast to the case for the bulks, only one resistivity peak was observed for the epitaxial LSMFO films. This shows that one of the two resistivity peaks for polycrystalline bulks has its origin in GB. The effect of Fe doping can be attributed to a combination of doping disorder, Fe–Mn superexchange interactions and a site-percolation mechanism. In epitaxial LSMFO thin films, the extrinsic MR related to the GB effect was excluded. The intrinsic MR is gradually enhanced with increasing Fe concentration. For the film with $x = 0.12$, a fairly large MR $= 12\%$ was observed in a small field of 4 kOe at 145 K. For such films, the resistivity above T_c follows the Emin–Holstein model for small polarons.

The polaron activation energy is enhanced due to weakening of the local DE ferromagnetism caused by Fe doping. The fitting results indicate that the lattice polarons are magnetic in nature and non-nearest-neighour polaron hopping occurs. The resistivity below T_p follows an empirical relation, $\rho(T, H) = \rho_0 + \rho_2(H)T^2 + \rho_{7.5}(H)T^{7.5}$. It is suggested that the enhanced MR arises from the suppression of the enhanced magnetic scattering and polaron scattering under an external field.

References

[1] Rao C N R and Raveau B 1998 *Colossal Magnetoresistance, Charge Ordering and Related Properties of Manganese Oxides* (Singapore: World Scientific)
[2] Hwang H Y, Cheong S W, Radaelli P G, Marezio M and Batlogg B 1995 *Phys. Rev. Lett.* **75** 914
[3] Zener C 1951 *Phys. Rev.* **81** 440
Goodenough J B 1955 *Phys. Rev.* **100** 564
[4] Li X W, Gupta A, Xiao G and Gong G Q 1997 *Appl. Phys. Lett.* **71** 1124
[5] Hwang H Y, Cheong S W, Ong N P and Batlogg B 1996 *Phys. Rev. Lett.* **77** 2041
[6] Balcells Ll, Fontcuberta J, Martinez B and Obradors X 1998 *Phys. Rev.* B **58** R14 679
[7] Ziese M 1999 *Phys. Rev.* B **60** R738 and reference therein
[8] Evetts J E, Blamire M G, Mathur N D, Isaac S P, Teo B S, Cohen L F and Macmanus-Driscoll J L 1998 *Phil. Trans. R. Soc.* A **365** 1593
[9] Liu J M, Huang Q, Li J, Ong C K, Wu Z C, Liu Z G and Du Y W 2000 *Phys. Rev.* B **62** 8976
[10] Uehara M, Mori S, Chen C H and Cheong S W 1999 *Nature* **399** 560
[11] Balcells Ll, Carrillo A E, Martinez B and Fontcuberta J 1999 *Appl. Phys. Lett.* **74** 4014
[12] Petrov D K, Krusin-Elbaum L, Sun J Z, Feild C and Duncombe P R 1999 *Appl. Phys. Lett.* **75** 995
[13] Liu J M, Huang Q, Li J, You L P, Xu S Y, Ong C K, Wu Z C, Liu Z G and Du Y W 2000 *J. Appl. Phys.* **88** 2791
[14] Ahn K H, Wu X W, Liu K and Chien C L 1996 *Phys. Rev.* B **54** 15 299
[15] Righi L, Gorria P, Insausti M, Gutierrez J and Barandiarán J M 1997 *J. Appl. Phys.* **81** 5767
[16] Leung L K, Morrish A H and Evans B J 1976 *Phys. Rev.* B **13** 4069
[17] Cai J, Wong C, Shen B, Zhao J and Zhan W 1997 *Appl. Phys. Lett.* **71** 1727
[18] Ogale S B, Shreekala R, Bathe R, Date S K, Patil S I, Hannoyer B, Petit F and Marest G 1998 *Phys. Rev.* B **57** 7841
[19] Chen X, Wang Z H, Cai J, Shen B G, Zhan W S and Chen J S 1999 *J. Appl. Phys.* **86** 4534
[20] Xianyu W, Li B, Qian Z and Jin H M 1999 *J. Appl. Phys.* **86** 5164
[21] Dominguez M, Bhagat S M, Lofland S E, Ramachandran J S, Xiong G C, Ju H L, Greene R and Venkatesan T 1995 *Europhys. Lett.* **32** 349
[22] Li J, Liu J M, Li H P, Fang H C and Ong C K 1999 *J. Magn. Magn. Mater.* **202** 285
[23] Kwon C, Robson M C, Kim K C, Gu J Y, Lofland S E, Bhagat S M, Trajanovic Z, Rajeswari M, Venkatesan T, Kratz A R, Gomez R D and Ramesh R 1997 *J. Magn. Magn. Mater.* **172** 229
[24] Boultif A and Louer D 1991 *J. Appl. Crystallogr.* **24** 987
[25] de Gennes P G 1960 *Phys. Rev.* **118** 141
[26] Coey J M D, Viret M, Ranno L and Ounadjela K 1995 *Phys. Rev. Lett.* **75** 3910
[27] Okuda T, Asamitsu A, Tomika Y, Kimura T, Taguchi Y and Tokura Y 1998 *Phys. Rev. Lett.* **81** 3203
[28] Snyder G J, Hiskes R, DiCarolis S, Beasley M R and Geballe T H 1996 *Phys. Rev.* B **53** 14 434
[29] Tiwari A and Rajeev K P 1999 *J. Appl. Phys.* **86** 5175
[30] Jonker G H 1954 *Physica* **20** 1118
[31] Tkachuk A, Rogacki K, Brown D E, Dabrowski B, Fedro A J, Kimball C W, Pyles B, Xiong X, Rosenmann D and Dunlap B D 1998 *Phys. Rev.* B **57** 8509
[32] Allub R and Alascio B 1997 *Phys. Rev.* B **55** 14 113
[33] Sheng L, Xing D Y, Sheng D N and Ting C S 1997 *Phys. Rev. Lett.* **79** 1710
[34] Sheng L, Xing D Y, Sheng D N and Ting C S 1997 *Phys. Rev.* B **56** R7053
[35] Emin D and Holstein T 1976 *Phy. Rev.* B **13** 647
[36] Sun Y, Xu X J, Zheng L and Zhang Y H 1999 *Phys. Rev.* B **60** 12 317
[37] De Teresa J M, Ibarra M R, Algarabel P A, Ritter C, Marquina C, Blasco J, Garcia J, Moral A D and Arnold Z 1997 *Nature* **386** 6622
[38] De Teresa J M, Ibarra M R, Blasco J, Garcia J, Marquina C, Algarabel P A, Arnold Z, Kamenev K, Ritter C and von Helmolt R 1996 *Phys. Rev.* B **54** 1187
[39] Hennion M, Moussa F, Rodriguez-Carvajal J, Pinsard L and Revcolevschi A 1997 *Phys. Rev.* B **56** 1187

[40] Sun J Z, Krusin-Elbaum L, Gupta A, Xiao G and Parkin S S P 1996 *Appl. Phys. Lett.* **69** 1002
[41] Chauvet O, Goglio G, Molinie P, Corraze B and Brohan L 1998 *Phys. Rev. Lett.* **81** 1102
[42] Worledge D C, Mieville L and Geballe T H 1998 *Phys. Rev.* B **57** 15 267
[43] Hundley M F, Hawley M, Heffner R H, Jia Q X, Neumeier J J, Tesmer J, Thompson J D and Wu X D 1995 *Appl. Phys. Lett.* **67** 860
[44] Schiffer P, Ramirez A P, Bao W and Cheong S W 1995 *Phys. Rev. Lett.* **75** 3336
[45] Mannari I 1959 *Prog. Theor. Phys.* **22** 335
[46] Campbell I A and Fert A 1982 *Ferromagnetic Materials* vol 3, ed E P Wohlfarth (New York: North-Holland) ch 9
[47] Thompson A H 1975 *Phys. Rev. Lett.* **35** 1786
[48] Kubo K and Ohata N 1972 *J. Phys. Soc. Japan* **33** 21